International Journal of Nanomedicine

Dovepress

open access to scientific and medical research

Open Access Full Text Article

ORIGINAL RESEARCH

RETRACTED ARTICLE: Anticancer Analysis of CD44 Targeted Cyclosporine Loaded Thiolated Chitosan Nanoformulations for Sustained Release in Triple-Negative Breast Cancer

Maisa Siddiq Abduh [1,2]

[1]Immune Responses in Different Diseases Research Group, Department of Medical Laboratory Scienc[illegible], Faculty of Ap[illegible]ed M[illegible]cal Sciences, King Abdulaziz University, Jeddah, Saudi Arabia; [2]Center of Excellence in Genomic Medicine Research, K[illegible]g Abdula[illegible] Univers[illegible]eddah, Saudi Arabia

Correspondence: Maisa Siddiq Abduh, King Abdulaziz University, Jeddah, Saudi Arabia, Tel +0[illegible]66568[illegible]8, Email m[illegible]bdoh@kau.edu.sa

Introduction: Cyclosporine (CsA), a potent immunosuppressive chemotherapeutic m[illegible]dication, treats numerous cancers, particularly malignant carcinoma, acute leukemia, and triple-negative breast cancer (TNBC).

Methodology: A specified polymeric nanoformulation (NF) base[illegible] drug delivery technique with ligand functionalization at the surface was developed to improve its delivery at the intended area a[illegible] boost the ef[illegible]acy for prolonged time. The in silico verified the HA binding to the CD44 receptor at binding sites A and B in triple-n[illegible]ative breast [illegible]ncer cells. The NF of encapsulated Cyclosporine in thiolated chitosan (TC) with the outermost coating of h[illegible]aluronic acid (HA) [illegible]s formulated and characterized.

Results: So, the zeta analysis revealed a particle size o[illegible]192 [illegible] and PDI of 0.433, zeta potential of 38.9mV. FTIR and Raman investigations also support the existence of hydrophobic g[illegible]roup[illegible] pore[illegible] surfaces, and non-clumping characteristics. While XRD verified its crystallographic nature while SEM [illegible] TEM a[illegible]ysis revealed the spherical nanoparticles with sleek exteriors. DSC demonstrated the stability of NF at high te[illegible]peratures. The NF showed 85% drug encapsulation followed Higuchi release model for therapeutic moiety at acidic pH for a maxi[illegible]m of 7[illegible] When compared to raw Cyclosporine, the in vitro tumor cell inhibition of ThC-HA encapsulated with Cyclosp[illegible]ne was [illegible]ed using an MTT dye on normal breast epithelial cells compared to triple-negative breast cancer cells.

Conclusion: This novel form[illegible]ation [illegible]proved the long-term viability, effectiveness, and active targeting as an effective and potent therapeutic moiety agains[illegible]ancer.

Keywords: breast ca[illegible]er, CD44, cyclosporine, hyaluronic acid, nanoformulations, triple-negative breast cancer, thiolated chitosan, targeted chemothera[illegible]utic dr[illegible] delivery

Intr[illegible]duct[illegible]n

Breast ca[illegible](BC) is the prevailing cancer among females. It is a multifaceted disease that encompasses several BC molecular su[illegible]pes and is generally characterized by the variation in the expression of membrane receptors. Triple-negative breast cancer (TNBC) is usually considered breast carcinoma, lacking all typical breast cancer receptors. TNBC comprises more than 25% of all BC, specifically in America, with a 56% convergence in gene expression studies, categorizing TNBC as a variant of basal-like BC.[1] TNBC has a more significant fatality progression of 40% in the chronic phase within the first five years after disease prognosis relative to other BC variants, and it typically manifests in young females. The average survival duration for patients with last-stage TNBC is not more than one year, and about 45% of them will acquire distant metastasis to the upper or abdominal organs.[2] Comparing TNBC to other subtypes of BC, therapeutic choices have generally been more constrained. Despite the advancement of novel biological and personalized medicines, cytotoxic chemotherapy continues to be the cornerstone of treatment for TNBC. Detailed

Received: 8 June 2023
Accepted: 30 September 2023
Published: 11 October 2023

information on the effectiveness of chemotherapeutic agents in the neoadjuvant, adjuvant, and metastatic contexts is available.[3] However, even though chemotherapy is the standard therapy against TNBC, the active therapeutic components employed could not distinguish between normal and cancerous cells. Numerous cancers, particularly malignant carcinoma, acute leukemia, and TNBC, are commonly treated with Cyclosporine (CsA), a strong immunosuppressive chemotherapeutic medication. However, due to P-glycoprotein-arbitrated efflux, its therapeutic potential exhibits poor solubility and rapid evacuation and generates adverse effects because of dose-limiting systemic toxicity.[4] This medication causes long-term harmful consequences to the heart, lungs, and kidneys while interfering with the morphological features of healthy cells that proliferate rapidly, including bone marrow, gastrointestinal cells, and hair follicles.[5]

Additionally, the therapeutic regimen for cancer typically necessitates delivering considerably high concentrations of chemotherapeutic medications with limited penetration to the injured tissues. A multimodal targeted drug delivery system (DDS) is employed to deliver the active moiety specifically to the malignant cells by minimizing the organ-based detrimental consequences and enhancing therapeutic effectiveness. Recently, ligand-modified nanoparticles (NPs) have obtained much surveillance in this area.[6] These pharmacological ligands can interact with particular receptors on the targeted cell surface, promoting functionalized nanoformulations' absorption.[7] DDS utilizes natural polymers and provides benefits over commonly employed pharmaceutical components. Localizing the medicine at the specified location and overcoming numerous biological impediments can improve bioactive chemical absorption and reduce organ-related toxicity.[8]

The presence of numerous functional groups for surface modifications makes biopolymers, including thiolated chitosan (ThC) coating with hyaluronic acid (HA), amiable and bioresorbable compounds.[9] Additionally, these polymeric composites possess covalently bonded free (active) thiol groups, they can bind to the surface receptors of the mucosal layer by covalent and non-covalent linkages, along with electromagnetic interactions and physical contrivance. Chitosan (Cs) is an ionized polymeric molecule derived from N-deacetylating chitin, strikingly identical to the naturally existing glycosaminoglycan.[10] The deacetylation rate affects the pharmacokinetic and pharmacodynamic attributes of this polymer. Moreover, Cs has an integral amine group (+NH2) which can be physiochemically manipulated. Physiological linkages with anionic substances found in the strands of other polysaccharides result in the production of covalent or ionic interactions, increasing Cs' magnetic strength.[11] The procedure, renowned as the "Ionic Gelation technique", depends on the electrostatic interactions in the presence of contrarily charged groups.[12] The benefits of this technology include the convenience of handling, the inclusion of biocompatible natural ingredients, and the uncomplicated regulation of particle size. The most frequently employed anionic crosslinked Cs is tripolyphosphate polyanion (TPP), a building block in fabricating commonly manufactured nanoparticles in personalized medicines.[13] The following steps are used by ThC when they have reached the targeted cell area: (i) Adhere to the dysfunctional polyp vessels. (ii) Inject the medicine in the capsule onto the targeted site. (iii) Directly bind the ligand to the receptors that have been increased on the cancer cell's membrane. (iv) Become ingested by the cancerous cells through receptor-arbitrated endocytic response. The outer layer, submucosal fluid, and connective tissues are all generally comprised of hyaluronic acid (HA), an aqueous mucopolysaccharide, composed of sequential molecules of N-acetylated sugar moieties.[14] This module contains operationally reactive sites, allowing biologically active components to interact. Moreover, the conjugation of suitable ligands, and other behavioral modifications, make them the perfect candidate for clinical use. Cell adherence, cancer progression, and propagation are all significantly influenced by the multifaceted, tumor-commencing CD44 cell surface receptor, which is overexpressed, particularly in advanced neoplasmic stages. The glycolytic pathway, reactive oxygen species, and the growth of TNBC cells have all been demonstrated to be under the control of CD44 in prior studies. A metabolic enzyme in TNBC cells, is necessary to regulate glycolysis and production of antioxidant species, assuring how quickly a tumor develops.[15] Because of its relatively greater binding affinity, HA attaches to CD44 receptors. The resulting ligand-receptor compound is then absorbed, which causes the polymer to degrade and releases the potent medicine into the target sites. DDS using HA polymers, the intrinsic ability of HA to bind with highly expressed CD44 membrane receptors, the primary binding receptor of HA on the surface of tumor cells, is reportedly being used to create nanoformulations with the encapsulation of pharmacologically active components. Due to the low penetration of HA into healthy tissues, the toxicities brought on by the lethal drug were decreased.[16] The primary objectives for the formulation of DDS with the inclusion of membrane-bounded ligands, ie, HA-coated ThC, were, therefore, to specifically target the neoplasmic areas by adhering to the CD44-R and to liberate potential nanomedicine by receptor-arbitrated endocytosis specifically at the malignant region (Figure 1).

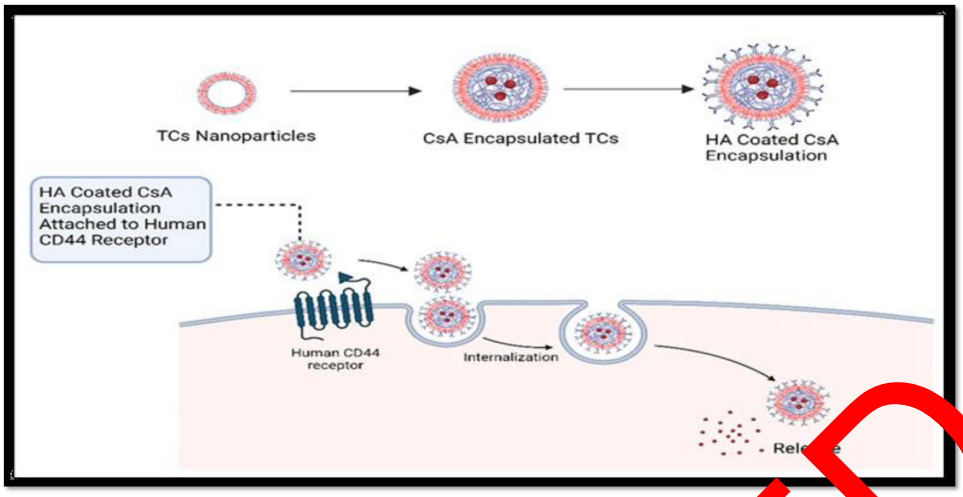

Figure 1 Localized delivery of CsA to triple-negative breast cancer cells by HA-coated ThC nanoformulation follo[illegible]g receptor mediate[illegible]d[illegible]tosis.

Materials and Methods

Chemicals and Reagents

Glacial acetic acid, N-hydroxy succinimide (NHS), Tripolyphosphate polyanion (TPP), Chitosan (Cs), and Thioglycolic acid (TGA) were taken from Quaid e Azam University, Islamabad, Pakistan. Hydroxylamine, Sodium dihydrogen phosphate, 1-ethyl-3-3 (3- dimethylamino propyl carbodiimide hydrochloride (EDC), Sodium hydroxide (NaOH), Calcium chloride ($CaCl_2$), Dipotassium hydrogen phosphate and Potassium dihydrogen phosphate were purchased from Merck (Germany). Artificial mucin, Hyaluronic acid (HA) (150 kD), High retention Dialysis membrane and Sodium borohydride were obtained from Scientific World traders. Quaid-i-Azam University, Islamabad, Pakistan, provided distilled water. Ellman's reagent (5, 5′-dithiobis-2-nitrobenzoic acid; DTNB) was supplied by Merck Traders. In this research, only an-analytical-grade chemicals and reagents were employed.

In silico Investigations

L-R Binding Through Molecular Docking

A protein data bank (PDB) classified as 4PZ3 was used to obtain the higher-resolution crystallized hierarchy of the normal human CD44 with HA-associated protein complex, while the structural configuration of HA was retrieved from the PubChem NCBI CID: 6452395 datasets. The PyMOL algorithm identified the two ligands (HA) associated with protein on 4PZ3 after all hydrophilic compounds had been eliminated. The PyRx 0.8, a visualization tool, was equipped with the biomolecule (4PZ3 receptor) and ligand. This software was coupled with Auto Dock Vina 4.2 to conduct the docking experiments. Binding energy values were used to evaluate the docking findings. Discovery Studio Visualizer, the L-R binding was employed to examine the molecular structure and interconnections between amino acids.

In silico Analysis for CD44 Expression

The expression of CD44 on breast cancer cells was analyzed using the GEPIA bio-informatics tool. GEPIA extracts data from GTEx (Gene-to-Tissue Expression) for normal tissues and TCGA (The Cancer Genome Atlas) for tumor tissues. The dot plot, box plot, overall survival, and disease-free survival data were extracted from GEPIA for CD44 expression in breast adenocarcinoma.

Synthesis of ThC

To make a ThC mixture, a previously published study by[9] was followed. Moreover, a milky, nebulous substance was produced after lyophilization and was kept at 4°C for future implications.[17]

Identification of Thiol (-SH) Groups on Chitosan

Using Ellman's solution, a sulfhydryl-containing water-soluble molecule, the disulfide bonds of ThC were detected. Due to the excellent reactivity of the solution at pH 7, it is employed for quantifying unbound sulfhydryl groups.[18] The ThC was mixed into the autoclaved H_2O, then 0.50 mL of phosphate buffer (PB) at pH-8.0 with Ellman's solution 0.5 mL, was added. The mixture was kept in an incubator for 2 hours at 25°C. The absorption was determined at a frequency of 420 nm after the biomolecular solution had been centrifuged at 23,500 rpm to collect residue. The control samples of Cs remained unchanged. The concentration of thiol compounds was estimated from the relevant control calibration curves developed against TGA standards.[18]

Synthesis of Nanoformulations of HA-Coated ThC

The ionic gelation technique was used to create the nanoformulations of the HA-encapsulated ThC. In all compositions, the addition of the ThC solubilized in de-ionized H_2O, and cross-linker TPP 0.1 mg/mL in ThC suspension, was then accompanied by the addition of HA in an aqueous medium. The nanoformulation was prepared to facilitate the bonding of crosslinked chemistry with the polymeric substances and cross-linkers.[19]

Synthesis of CsA Encapsulated Drug in Nanoformulation

The ionic gelation approach produced the CsA encapsulated nanoformulation with minor adjustments. The nanoformulations of varied concentrations were produced by adding 0.1 mL TPP and continuously stirred at 550 rpm for 15 minutes. Then, for 15 minutes, all of the compositions were sonicated at 30 mA. The finalized mixture was centrifuged, lyophilized, and encapsulated with 1 mg/mL HA.[18]

Optimization of a Nanoformulation Synthesis Protocol

Using DesignExpert software, the BoxBehnken factorial design for nanoformulation refinement was used to select the core component architecture. The encapsulation efficiency (EE), zeta potential (ZP), polydispersity index (PDI), and nanoparticle size (NPS) were the key determinants that were evaluated (Table 1). Finally, an optimal composition was chosen, and characterization features were assessed.

Table 1 For Improving NF, Features Run on DOE Encompass Varying HA and TC Concentrations with Changing Sonic Radiation Time, Particle Size, Zeta Potential with PDI

Run	HA mg	TC mg	CysA mg	Particle Size nm	PDI	Zeta Potential ±mV
1	50.00	20.00	17.50	1444	1	−9.84
2	50.00	100.00	17.50	752.8	1	10
3	25.00	60.00	25.00	460.7	0.49	25.6
4	37.50	20.00	25.00	387.2	0.591	−23.7
5	50.00	60.00	25.00	390.12	0.162	17.1
6	37.50	20.00	10.00	293	0.42	−22.5
7	37.50	100.00	25.00	1683	1	7.5
8	25.00	20.00	17.50	396.2	0.524	−27.6
9	37.50	60.00	17.50	416.7	0.584	12
10	25.00	100.00	17.50	3191	1	10
11	50.00	60.00	10.00	438	0.678	12
12*	**25.00**	**60.00**	**10.00**	**192.5**	**0.433**	**38.9**
13	37.50	100.00	10.00	2133	1	6.5

Note: *The red colored parameters were selected for the formulation of nanoparticles.

Characterization of Nanoformulations

The efficacy of nanoformulations as a potential treatment element was assessed by characterizing their numerous features.

Physiochemical Attributes of Nanoformulations

Malvern Zetasizer Nanos ZS90 was used to measure the average NPS, PDI, and ZP of blank and CsA encapsulated nanoformulations. The measurements were made with the nanoformulations dissolved in autoclaved H_2O at a ratio of 1:10 at room temperature. Three distinct batches were examined for the average NPS, PDI, and ZP to determine an average value.

Morphological Attributes of Nanoformulations

SEM was used to examine the morphology of ThC-HA nanoformulations that were empty and loaded with CsA (TESCAN, Czech Republic). The aluminum stubs were filled with a tiny amount of lyophilized powder with a gold coating. The SEM images were captured using electrons that were intensified with 15 kvolts.[9]

Determination of Functional Group of Nanoformulations

To identify the constituents in prepared nanoformulations, the Fourier transform infrared (FTIR) technique was employed and ascertain their functional groups.[9] The lyophilized powder of nanoformulations was utilized to identify the functional group's distinctive peaks.[21]

Crystallographic Investigation of Nanoformulations

Using an alpha-radiated D8 ADVANCE X-ray diffractometer (Bruker, Germany), the crystalline quality of lyophilized blank and CsA encapsulated nanoformulation was assessed by following the protocol of.[17]

Surface Investigation of Nanoformulations

The surface of NF and Raman spectroscopy, a scattering and non-destructive biochemical technique, examined CsA encapsulated nanoformulations. With a laser power of 150 mW and an activation frequency of 780 nm, the empirical data processing frequency range was 0–3500 cm^{-1}. The same variables were used to acquire all spectral information. Like FTIR, it uses the interaction of light with a substance to learn more about a molecule's composition or properties. Moreover, the scanning range used to create the spectra was 200 to 2000 cm^{-1}.

Thermal Stabilization of Nanoformulations

Differential Scanning Calorimeter (DSC) (USA) measurements were made to determine whether blank and CsA encapsulated nanoformulations were stable at high temperatures. A sample is subjected to a constant temperature by using a thermal analysis approach, which measures the rate of heat flow into or out of the samples due to time or temperature.

CsA Loading and Encapsulation Efficiency (EE) %

An indirect approach was employed to calculate the proportion of CsA enclosed in nanoformulations. After centrifugation, a syringe filter was used to collect the supernatant and then subjected to an additional Ultraviolet-Visible (UV-Vis) spectrophotometer (NanoDrop 2000c, USA) analysis at 269 nm to examine the presence of a free drug. The formulas employed in our previous studies[9] were used to estimate the EE and DL ratios.[20]

In-Vitro CsA Release Study of Nanoformulations

Dialysis bag submerged in PB pH 6.8 and 7.4 at 37oC to assess the release of Cyclosporine from nanoformulations. The dialyzing membrane was filled with 5 mg of lyophilized powder, and 50 mL of PB in both pH ranges, and a magnetic hot plate was used to keep the dissolution media warm. The release of readily accessible Cyclosporine was also assessed

using the same methodology for comparison purposes. Triplicate samples were used in the investigation. A UV-Vis spectrophotometer (NanoDrop 2000c, USA) was used to evaluate the samples (1.5 mL) at 269 nm at predetermined intervals of 0, 2, 12, 24, 48, and 72 hours. The standard calibration curve of Cyclosporine at pH 6.8 and 7.4 in phosphate buffer was used to calculate the findings[9] and display them on an Excel spreadsheet.[22]

Dynamics of Cyclosporine Release

A key element in establishing a dosage therapeutic effect is how the molecule is released from the matrix. Various kinetic methods were utilized for in-vitro Cyclosporine release and nanoformulations penetration to elucidate the process of drug release from nanoformulations.[17]

Zero-Order Kinetics

The graph between the cumulative release of CsA versus time was constructed to analyze its kinetic of release following zero-order by ensuing the protocol provided by.[9]

First-Order Kinetics

The optimum sink conditions were retained in these circumstances, as explained by first-order kinetics. The previously selected formula was employed to construct the cumulative values for the drug release log against time on the graph.

Erosion Model (Hixon Crowell's Cube Root Equation)

Drug release is illustrated by various methods in Hixon Crowel's model, including erosion and diffusion. The formula applied to this model was like the[9] study.

Diffusion/Relaxation Model (Korsmeyer Peppas or Power-Law Equation)

This concept is demonstrated by the formula reported by,[9] which plots drug release against time using an exponential curve.

In-Vitro Antitumor Efficacy of Nanoformulations of CsA Encapsulated Nanoformulations

Cell Culture

In contrast to raw Cyclosporine, the in-vitro antitumor activity of nanoformulations of CsA (CsA-NF) encapsulated ThC-HA was assessed employing normal breast epithelial cells (MCF-10A) and triple-negative breast cancer cells (MDA-MB-231) by following the protocol of.[9] In-vitro antitumor potential was analyzed using three assays: MTT, trypan blue exclusion assay, and cell morphology analysis. When the cells reached the exponential curve phase, they were used for further investigations after being cultured in 75 cm^2 tissue culture flasks.[23]

In-Vitro Experimental Groups

The six groups were developed for an in-vitro investigation using breast cells:

1. Group 1: Control MDA-MB-231 in RPMI
2. Group 2: Inj.CsA-treated MDA-MB-231 cells
3. Group 3: CsA-NF-treated MDA-MB-231 cells
4. Group 4: Control MCF-10A cells
5. Group 5: Inj.CsA-treated MCF-10A cells
6. Group 6: CsA-NF-treated MCF-10A cells

MTT Assay for Cell Viability

The previously published approach was used to determine the cytotoxicity of CsA-NF with a few minor adjustments. The cells were seeded in 96-well plates at a cell density of 1×10^6 cells/ well and incubated in appropriate conditions to grow until the appropriate confluence rate was reached. Five separate groups were made by following the protocol.[9] The normal breast epithelial cell line and TNBC cell line were used for the comparative analysis of the findings of CsA

encapsulated in nanoformulations and the raw format of the CsA.[24] After 24 hours, the medium was withdrawn from the cells, and then various concentrations of CsA-NF and blank were applied by following the protocol provided by.[9]

Trypan Blue Exclusion Assay for Cell Viability

Membranes of living cells are intact, whereas dead cells have perforated membranes because of which they retain trypan blue dye while living cells do not. Trypan blue exclusion assay is performed to quantify the number of living/dead cells in a suspension.[9] The cell viability was determined by using the formula.

% Viability of cells = Viable cell count x 100
Total number of cells

Cell Morphology Assay for Cytopathic Effect

To determine the apoptotic effects of pure CsA and CsA NF, cell morphology analysis was done by treating both cell lines with different concentrations of pure drug and NF and then analyzing the cellular morphology associated with apoptotic effects. The hallmarks of apoptosis include rounding, aggregation, detachment (for adherent cells), blobbing, and shrinkage. For this purpose, both normal and cancerous cell lines (MCF-10A and MDA-MB-231) were seeded at 1×106 cells/well density in a 96-well plate at 37°C in a CO2 incubator. After 24 hours, the cells were exposed to CsA and CsA-NF at different concentrations (10, 40, and 80 µg/mL dissolved in PBS). A phase contrast microscope was used to observe changes in cell morphology post-24 hours of cell treatment.

Stability Analysis

The stabilization of the nanoformulations of CsA encapsulated in HA was examined over three months while being maintained at 4°C and room temperature of 37oC for changes in particle size, PDI, zeta potential, and shape. Before an assessment, the nanoformulations were re-distributed into deionized water after being stored in lyophilized form.

Statistical Evaluation

With a significant p-value of less than 0.05, one-way analysis of variance (ANOVA) and Student's *t*-test was used to statistically analyze the data, which were then given as the mean of three samples plus standard deviation (mean + SD).

Results and Discussions

Molecular Docking

The AutoDock Vina feature in the PyRx software was used to conduct the docking experiments of HA. PDBQT file format was used to save the structural confirmations. To accomplish docking through the AutoDock Vina tool, these systems were uploaded in the graphical interface panel, grid pane, and grid box, and the box attributes were adjusted appropriately. The peptide receptor has two adhesive domains, A and B; each was docked with HA, and generated results were quite comparable. The binding affinity was determined as 7.1 and 7.0 kJmol-1 for citing A and B, respectively, was used to assess the intensity of the binding contract between the ligands (HA) and the peptide receptor (4PZ3)[25] as shown in Figure 2.

In silico Analysis for CD44 Expression

After comparing normal tissue data (from GTEx), and tumor tissue data (from TCGA). GEPIA analysis outcomes showed that CD44 is highly over-expressed on breast adenocarcinoma tissues as compared to normal breast tissues, as shown in Figure 3 dot plot (A), box plot (B), and role of CD44 expression on breast adenocarcinoma patients' overall survival and disease-free survival (C). Unlike overall patient survival, CD44 expression was very prominent in patients' disease-free survival after treatment with chemotherapeutic drugs.

Optimization of Nanoformulations

Using DesignExpert updated variant, the BoxBehnken factorial design for the refinement of nanoformulation was used to select the core component structure (Figure 4). The NPS, PDI, ZP and EE were the variables that were examined as

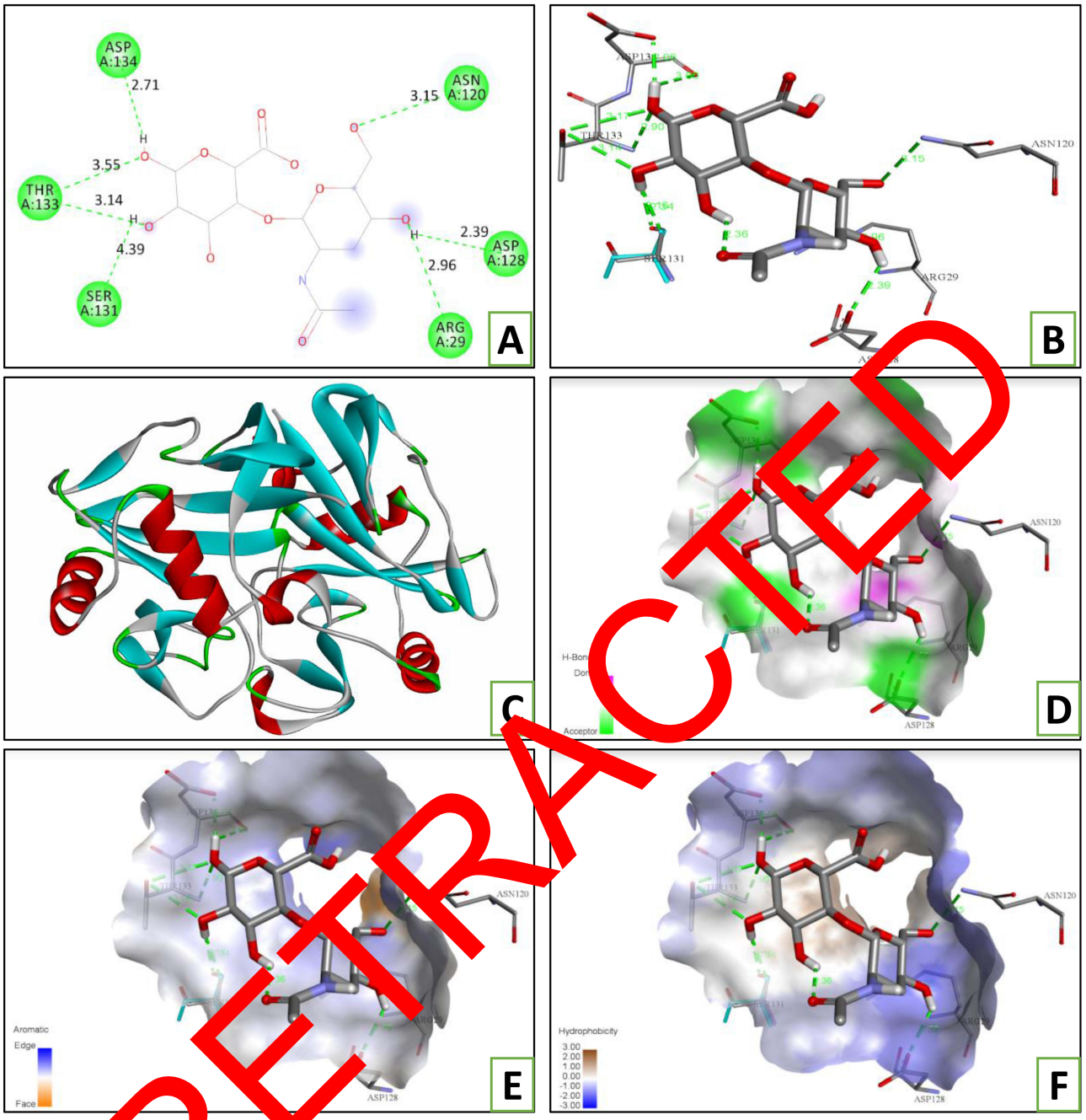

Figure 2 2D (**A**) and 3D (**B**) structure of hyaluronic acid (ligand) downloaded from PubChem NCBI database and CD44 (4PZ3) receptor downloaded from protein data bank (**C**). 3D-Ligand H-bonding (**D**) 3D-Ligand aromatic-bonding (**E**) 3D-Ligand hydrophobic bonding (**F**) by using Discovery studio 2017 R2 Client. The Green dashed line represents H-bonds; the red line represents an unfavorable bond in part A.

dependent variables. Finally, as illustrated in Table 1, an optimal formulation was chosen, and qualitative features were assessed.

Synthesis of Nanoformulations of Blank and CsA Encapsulated ThC-HA

There were 850 µMol/g of thiol groups in the polymer. By employing the cross-linker TPP, the positively charged amino group of ThC and the negatively charged HA inter-acted ionically to produce the nanoformulations of the blank, and CsA encapsulated ThC-HA. In a process involving sodium tripolyphosphate, glacial acetic acid, and 0.1 mg/mL quantities of Cyclosporine, the ThC mixture was disintegrated, producing nanoformulations of Cyclosporine encapsulated ThC-HA. In

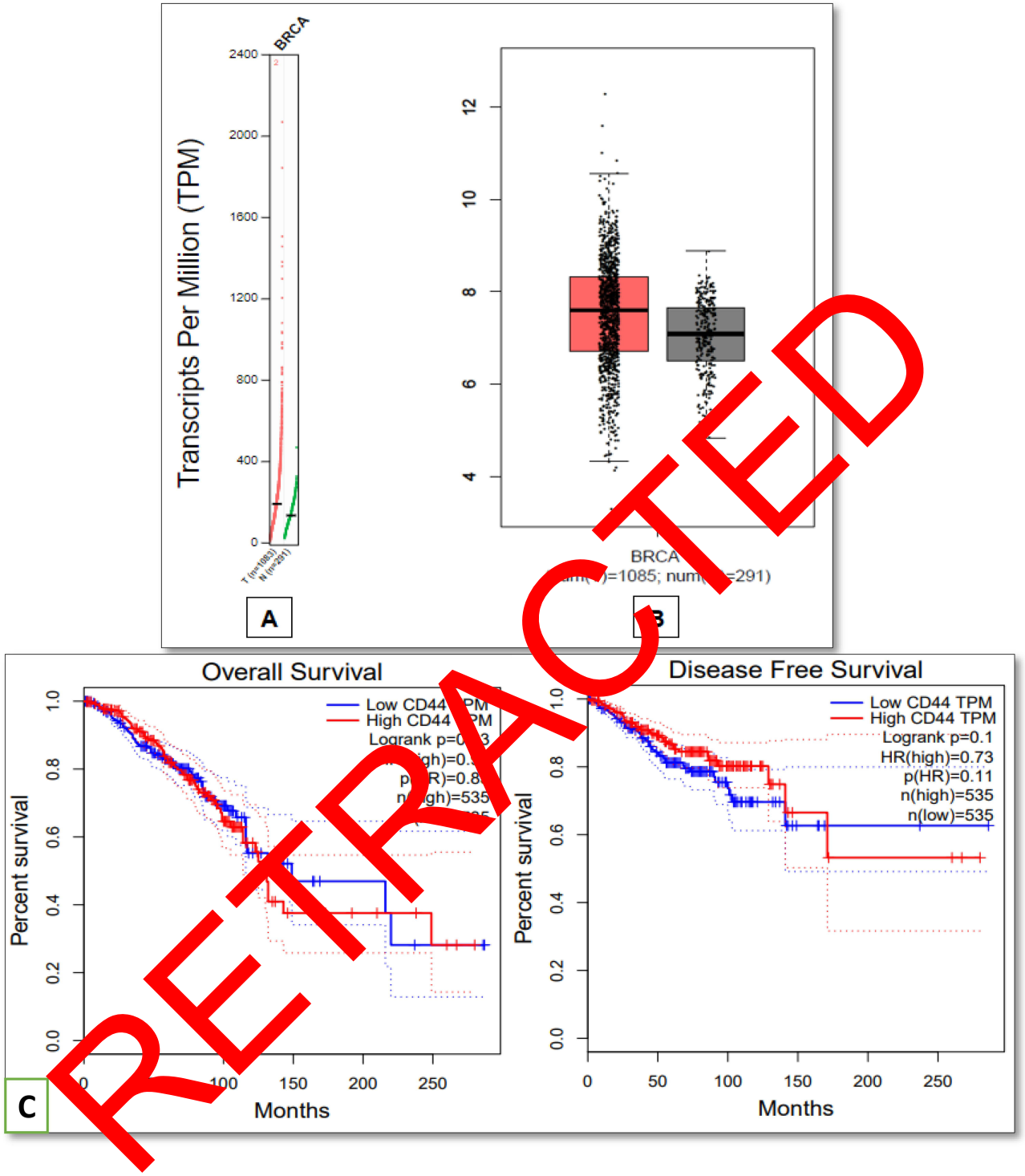

Figure 3 Dot plot (**A**) and Box plot (**B**) data for CD44 expression in breast adenocarcinoma and normal breast tissues (**C**) Effect of CD44 expression on overall survival and disease-free survival post-treatment. X-axes indicate survival time in months, while Y-axis indicates the percent survival of patients.

prior studies, the ionic gelation process was used to create methotrexate-encapsulated Cs nanoparticles tested in vitro against the LNCaP cell line.[26] A related method was used to assess the cytotoxic effects of VC-encapsulated folic acid-Cs linked nanomaterials on NCI-H460 cells.[27]

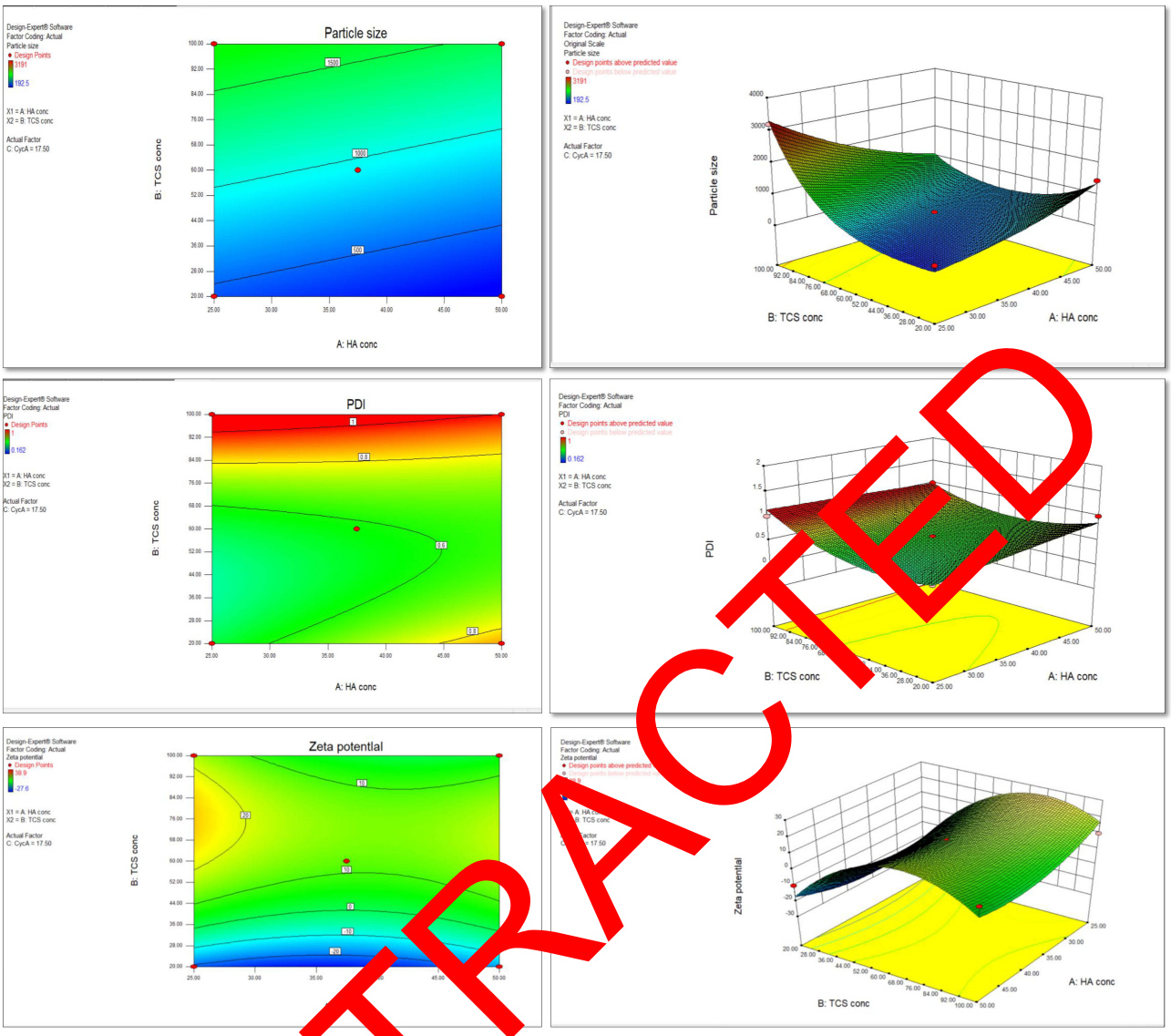

Figure 4 Zeta potential, particle size, and PDI, consideration in a Box-Behnken factorial design using DOE for the optimization of NF.

Characterization of Nanoformulations

Physiochemical Attributes of Nanoformulations

Zeta sizer was used to examine the size distribution and PDI of the nanoformulation, and the findings of modified nanoformulations of blank and Cyclosporine encapsulated with ThC-HA are depicted in Figure 5 and Table 2. Triplicate measurements were taken to calculate mean results. For blank nanoformulation, the average smallest NPS was 184.9 nm with a ZP of 37 mV and a PDI of 0.428 at a level of 60 mg/mL ThC. The average NPS and ZP of nanoformulations of CsA encapsulated ThC-HA, on the other hand, increased with increasing polymer content from formulations with unchanged drug levels. The zeta potential of the smallest size of CsA encapsulated nanoformulations was 192.9, and the PDI was 0.433 at a rate of 60 mg/mL ThC.[28] Numerous factors, primarily the particulates' size, shape, surface charge, and cytotoxicity, impact nanoformulations' effectiveness.[23] The structural and physiochemical characteristics of the NPs were examined.[29]

Additionally, NPs smaller than 300 nm have a substantially longer dissolution rate due to limited reticuloendothelial system absorption, which has resulted in a rise in malignant cell uptake. For DDS targeting cancer cells, nanoformulations of CsA encapsulated ThC-HA smaller than 300 nm can be employed. According to a study, charged NPs were eliminated from the body's circulation more quickly than uncharged ones, and formulations with positive ZP encouraged the absorption of NPs by tumor cells. A recently published research revealed the usage of preactivated ThC NPs encapsulated with octreotide that had a peak

Figure 5 NFs of Blank particle size and PDI (**A**), zeta potential (**B**) and CsA-loaded ThC-HA particle size and PDI (**C**), zeta potential (**D**).

performance of octreotide (89 ± 6% and showed a mean NPS of 277 ± 19 nm, 0.2 PDI and ZP of +28.2 ± 3 mV.[30] The nanopowder ThC-HA and isoniazid for inhalation were published in another research.[31] They have physical and chemical characteristics, including zeta sizes of 300.2 ± 2.3 nm and 342.1 ± 18.8 nm, respectively. Drug loading, drug solubility, bioavailability, in vivo diffusion, and product durability are all affected by nanoformulations in some way. These effects rely on the particle diameter, charge, and distribution of the particles.[32] Because they attach to the edge of the particle surface, the smaller NPs have a high surface-volume ratio, are instantly aggregated, and are released quickly. Comparatively, to neutral and negatively charged NPs, positively charged NPs exhibit greater uptake through direct absorption.[33]

Morphological Attributes of Nanoformulations

The surface form, and size of the nanoformulations of blank and CsA encapsulated in ThC-HA were confirmed using SEM and TEM examination. Regardless of the various delivery methods, the morphology significantly affects the movement and dispersion of NPs within the cell.[33] The results indicated the formulation's smooth surface particles, as illustrated in Figure 6A. These

Table 2 Physiochemical Properties NFs of Blank and CsA-Loaded ThC-HA s Were Negatively Charged

Sr. No	Formulation	Particle Size (nm)	PDI	Zeta Potential (mV)
1	Blank NF	184.9	0.428	37.8
2	CsA-loaded ThC-HA	192.9	0.433	38.9

graphics somehow resembled one another due to the drug being loaded correctly inside the polymeric substance. The lyophilized, circular nanoformulation of CsA encapsulated in ThC-HA was seen in the TEM images (Figure 6B).

Curcumin-encapsulated N, O-carboxymethyl Cs NPs were also discovered to have a circular form, and their antitumor efficacy was assessed against L929, and MCF-7 cell lines.[34] Research reported that ferulic acid encapsulated Cs NPs had substantial antitumor efficacy against ME-180 and confirmed their uniform and circular structure.[34] When employed against NCI-H460, the CsA encapsulated folic acid-Cs coupled NPs had a suitable antitumor property and had a circular form with a uniform surface.[27] Previous research has shown that the particle's morphology and structural confirmation significantly impact intracellular delivery. Due to their intrinsic configuration, the circular particles readily absorb the bloodstream.[35]

Functional Group of Nanoformulations

When comparing the formulations with HA and ThC in the lyophilized form to the blank and CsA encapsulated formulation, the FTIR spectrum revealed distinguishing peaks and data regarding the structure and phase composition (Figure 6C). The primary TC lines were detected at 3400^{-1} due to the bending of the OH, CH, C-O, and C2 bond at 2940 cm^{-1} respectively linked to the CN bond.[36] Moreover, the -SH bending peak at 1650 cm^{-1} additionally verified the existence of thiol groups. The research found that mucoadhesive thiomeric Cs nanoparticles synthesized for the selective ocular delivery of Cyclosporine exhibited identical peaks.[17]

Crystallographic Investigation of Nanoformulations

XRD analysis was used to determine the implications of intramolecular and extra-molecular associations on the crystallized structure of nanoformulations of CsA-encapsulated ThC-HA. The significant reflection was seen at $2\theta = 15.2^{\circ}$ in CsA encapsulated nanoformulation in Figure 7A. These findings showed that CsA encapsulated ThC-HA had a high crystallinity level that was very close to that of blank nanoformulations due to the formation of hydrogen bonds between molecules and extra molecular forces that may have persisted in the CsA encapsulated formulation as well. To comprehend the crystalline morphological conformation of crystalline and semi-crystalline materials, X-rays are

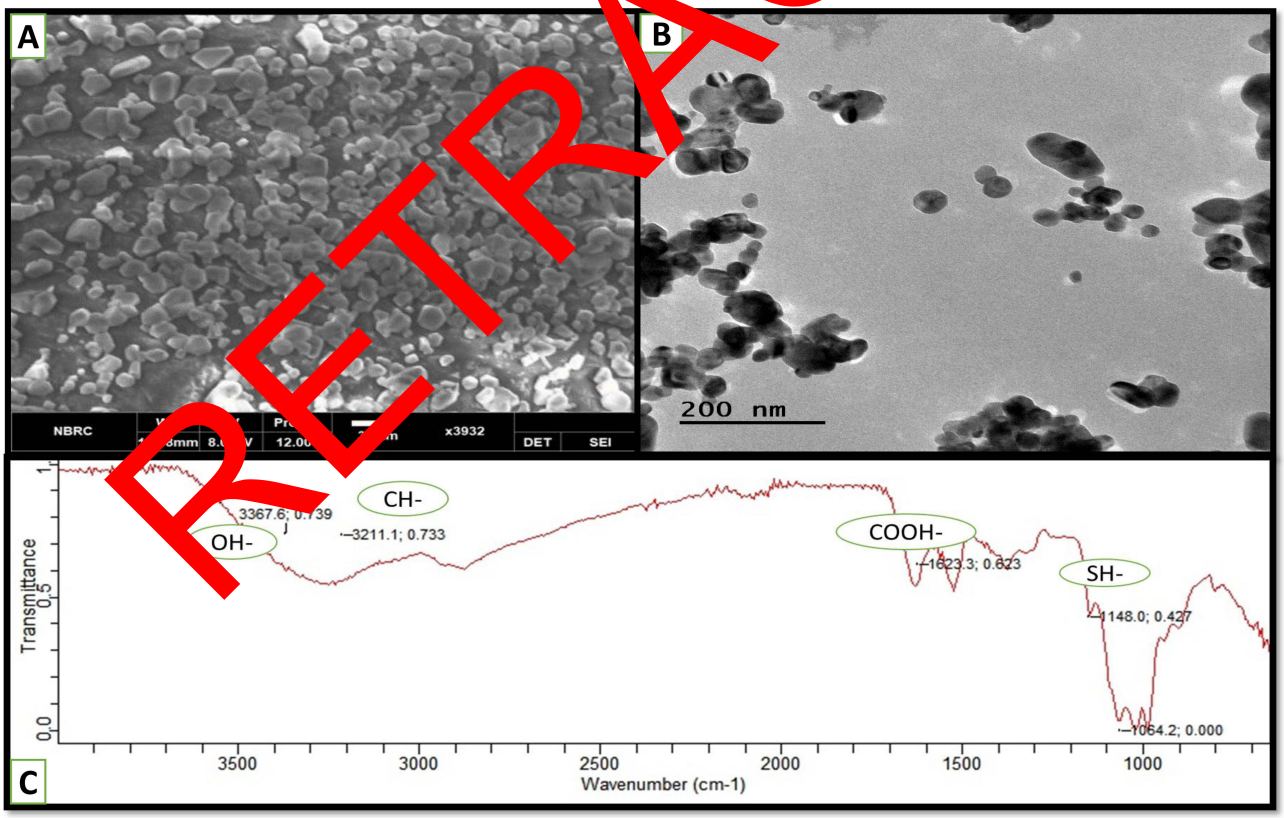

Figure 6 SEM images of a plane surface with nanosize, smooth and spherical shaped nanoparticles at 3μm (**A**) CsA-loaded ThC-HA, and (**B**) TEM showed more precise image of NF at 200nm exhibiting spherical granules. There shape support their movement in the leaky vasculature of cancer cells (**C**) FTIR spectrum of nanoformulation of CsA-loaded in ThC-HA.

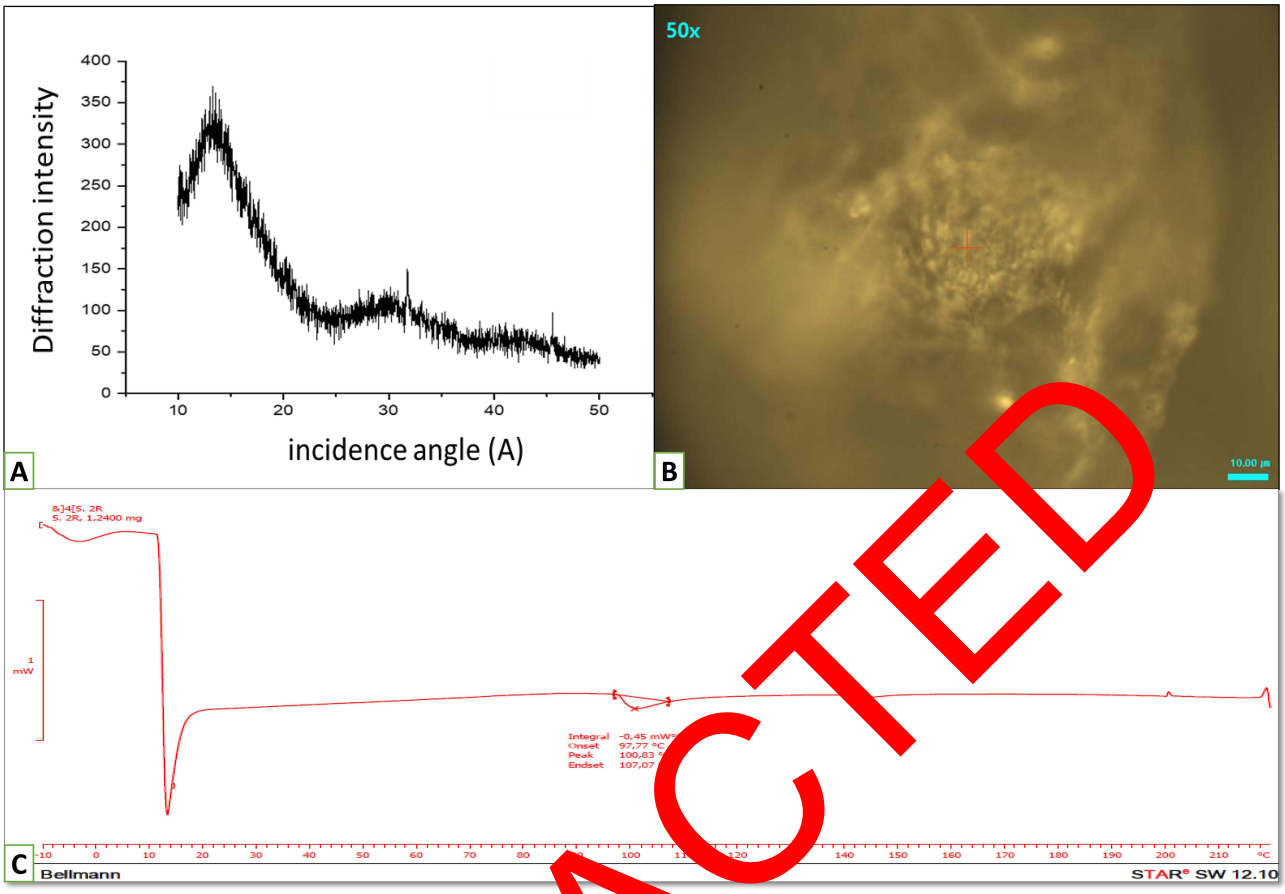

Figure 7 XRD analysis showed the amorphous nature (**A**), Raman analysis showed the porous surface of NFs (**B**) and DSC thermogram of NF of CsA-loaded in ThC-HA.

dispersed by a periodic arrangement of atoms, which generates discrete diffraction peaks that give a qualitative depiction of the elemental composition within the crystalline lattice.[31]

Surface Analysis of Nanoformulations

Figure 7B shows the Raman spectroscopy results for the nanoformulations of CsA-encapsulated ThC-HA. This result demonstrated that nanoformulations have porous surfaces due to their aggregation properties, making them ideal for DDS.[37]

Thermal Stabilization of Nanoformulations

The dehydrating temperature (TD) attributed to the loss of water linked with the hydrophilicity of ThC, was visible in the DSC thermal images of the nanoformulations of CsA encapsulated in ThC-HA. The deterioration of the polymeric substances was shown by an exothermic peak that rises between 140 and 190oC. Thermogram results revealed that the nanoformulations of the CsA encapsulated ThC-HA showed more excellent stabilization than the Cyclosporine drug currently available. According to the DSC thermograms, adding thiol groups to Cs improves its overall stability, improving the reliability of the nanoformulations generated by entrapping the drug in this polymer, as seen in Figure 7C. Considering the alteration of Cs to produce thiolated chitosan and stability enhancement at elevated temperatures,[17] reported similar results previously.

Cyclosporine Loading and Encapsulation Efficiency (EE) %

UV-Vis spectrophotometer was used to calculate how much loaded Cyclosporine was in the nanoformulations. According to Table 3, the average percentages of EE and DL of nanoformulations of CsA encapsulated ThC-HA were 85% and 14%, respectively. Prior studies on the drug-loaded nanoformulations revealed a higher pharmacological profile and improved efficacy in-vivo and in-vitro investigations.[38] Gemcitabine was previously shown to have 3.91 ± 0.12 DL and EE 85.4 ± 4.9% in folic acid-Cs linked NPs.[39]

Table 3 Percentages of EE and DL NFs of CsA-Loaded in ThC-HA

Absorbance	Encapsulation Efficiency (EE%)	Encapsulation Efficiency % (Mean ± SD)	Drug Loading (DL)	Drug Loading % (Mean ± SD)
2.9031	85.35%	85.70%±0.0031	14.32	14.27±0.05
2.818	85.78%		14.22	
2.781	85.97%		14.29	

In vitro Cyclosporine Release Study

The drug release test was carried out using a dialysis bag submerged in PB pH 7.4 and 6.8 at [illegible]°C to assess the release of Cyclosporine from nanoformulation. Table 4 and Figure 8A display the time-dependent mean of percentage Cyclosporine release, demonstrating that the drug from nanoformulation is released in PBS pH 7.4 within 72 hours. However, the drug release from nanoformulations was approximately 85% in an acidic medium, a relatively better but continuous release after three days. Multiple doses of standard chemotherapeutic medicines are needed to attain the plasma levels in the blood circulation because the Cyclosporine was released at pH 7.4 and the residual was released immediately in 24 hours[40] and previously stated that the encapsulated medicines were released slowly in a similar fashion. In simulated gastric juice with a pH of 1.2 and intestinal fluid with a pH of 6.8, the study demonstrated a delayed release of mi-mitoxantrone-encapsulated folic acid-Cs linked NPs. Another investigation on VC-loaded folic acid-Cs linked nanoparticles revealed 5.51% slow and persistent release of VC of 4:25 formulation within 2 h s, and subsequent release was 5.47, 5.57, and 11.11% after 4, 6, and 8 h s, respectively.[27] The polymer's concentration and the medication's release were shown to be inversely related. The drug release was shown to be delayed by all formulations for up to 12 hours.

Dynamics of Cyclosporine Release

Various kinetic parameters were used to develop the drug release process using the information of the cumulative % of drug release at pH 7.4 and 6.8 in the designated time frames, as reported in Table 5. The Higuchi diffusion approach was deemed the best compared to all kinetic models at pH 7.4, and 6.8, as shown in Figure 8B and C, because their R2 values

Table 4 Drug Release Rates from Synthesized NF and Unprocessed CsA at Predetermined Intervals in Phosphate Buffers at pH 7.4 and 6.8, Respectively

Sr. No.	Time (Hr)	Absorbance (pH 7.4)	Absorbance (pH 6.8)	% CsA Released from Nanoformulation at pH 7.4 (Mean ± S.D)	% CsA Released from Nanoformulation at pH 6.8 (Mean ± S.D)	Drug (CsA) Solution at pH 7.4 (Mean ± S.D)
1	0	0		0	0	0
2	0.5	0.123	0.1064	7.779119	26.75053467	7.779119206
3	1	0.1122	0.11274	15.54774	55.2900819	15.54774028
4	2	0.1101	0.13092	23.0959	62.20910204	23.09590048
5	4	0.1041	0.14143	30.01417	70.3048071	30.01417248
6	6	0.1038	0.15731	36.90095	77.7515013	36.90095008
7	12	0.1028	0.15268	43.68275	80.92601096	43.68274631
8	24	0.1109	0.15983	51.31489	81.63710112	51.31489161
9	48	0.1127	0.16245	66.15926	84.39398639	59.13600336
10	72	0.246	0.16809	80.19526	86.72478192	66.15925673

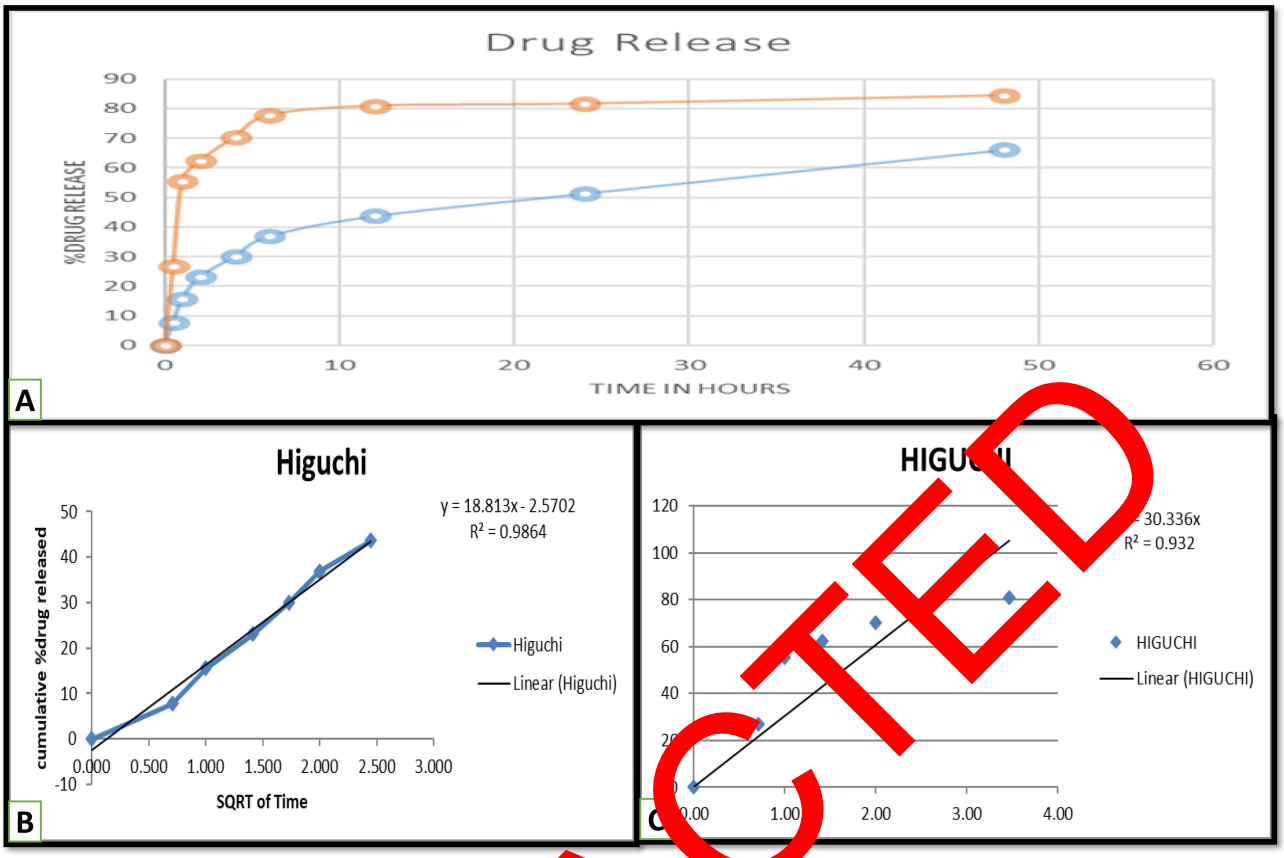

Figure 8 Drug release at pH 7.4 and 6.8 from CsA nanoformulation (**A**), Higuchi graphical release model for drug release of CsA-loaded in ThC-HA at pH 7.4 (**B**) and 6.8 (**C**).

were near to 1 and demonstrated drug release by a streamlined diffusion method. The rate of drug release (R2) and k (slope) values obtained for all kinetic parameters are depicted in Table 6. Because the network model of the nanoparticles is stable at this pH, the drug release is relatively low. These findings align with an earlier study that investigated polypeptide drug release from CS-CS nanoparticles for colon targeting and found that the process is pH dependent.

Table 5 Determine the Optimum Kinetic Model Using Percentages of Drug Release in Phosphate Buffer pH 7.4 at Predetermined Time Intervals

Sr. No.	Time (Hr)	Cumulative % CsA Released (pH 7.4)	Cumulative % CsA Released (pH 6.8)
	0	0	0
2	0.5	7.779119	26.75053467
3	1	15.54774	55.2900819
4	2	23.0959	62.20910204
6	4	30.01417	70.3048071
7	6	36.90095	77.7515013
8	12	43.68275	80.92601096
9	24	51.31489	81.63710112
10	48	66.15926	84.39398639
11	72	80.19526	86.72478192

Table 6 The Different Kinetic Models on Drug Release of NFs at pH 7.4 and 6.8

	Zero-Order		First-Order		Higuchi		Korsmeyer-Peppas		Hixon Crowell	
	R^2	K_1	R^2	K_2	R^{2*}	K_4	R^2	K_5	R^2	K_3
pH 7.4	0.9389	7.137	0.9712	−0.0413	**0.9864**	18.81	0.5902	10.263	0.6753	0.423
pH 6.8	0.6794	10.535	0.7212	−0.0526	**0.932**	30.33	0.2554	0.7071	0.6579	0.1373

Notes: *R2 (highlighted) value close to 1 is th eindicator of best kinetic model followed by release of drug from formulations.

In-Vitro Anticancer Potential of CsA-NF

MTT Assay for Cell Viability

The anticancer potential of CsA-NF was tested on MCF-10A and MDA-MB-231 at concentrations of 20, 40, and 90 µg/mL and contrasted to raw Cyclosporine (Figure 9). When the drug concentration is increased from between 20 and 90 g/mL, it has a dose-dependent effect on the cell survival of MCF-10A cells that have been exposed to CsA and CsA-NF. MDA-MB-231 cells, when treated with pure CsA, the highest cell viability of 70.90±0.04% was observed at a concentration of 20µg/mL, and the lowest cell viability of 34.8±0.03% was observed at a concentration of 90 µg/mL, as reported in Figure 9 with an IC50 value of 45.2±0.04%. Moreover, CsA-NF significantly reduces the viability of normal breast cancer cells MDA-MB-231. At 20µg/mL, it was 66.90±0.03% but when the nanoformulation concentration was raised to 90 µg/mL, it was only 20.87±0.01%. The IC50 for CsA-NF was 40.1±0.02 µg/mL for MDA-MB-231. MCF-10A cells, when treated with pure CsA, the highest cell viability of 31.98±0.03% was observed at a concentration of 20µg/mL, and the lowest cell viability of 14.39±0.03% was observed at a concentration of 90 µg/mL, as reported in Figure 9 with an IC50 value of 25.3±0.04%. Moreover, CsA-NF demonstrates less significant reduction in the viability of normal breast cancer cells MCF-10A. At 20 µg/mL, it was 44.7±0.03%, but when the nanoformulation concentration was raised to 90µg/mL, it was only 65.41±0.02%. The IC50 for CsA-NF was 65.1±0.02 µg/mL for MCF-10A. Therefore, as seen in Figure 9, the synthesized NF is less toxic to normal breast cancer cells than the conventional Cyclosporine, whereas it is highly cytotoxic to cancerous cells compared to pure CsA.

Trypan Blue Exclusion Assay for Cytotoxicity

Trypan blue exclusion assay helped us to evaluate the cytotoxic potential of pure CsA and CsA-NF at different concentrations of 10, 40, and 80 µg/mL. As shown in Table 7 below, % cytotoxicity increased with increased concentration of NFs. For MDA-MB-231 cells, maximum % cytotoxicity of 79.2±0.07% was observed at a concentration of 80µg/mL, and minimum cell viability of 11±0.04% was observed at a concentration of 80 µg/mL for pure CsA treated cells. For MCF-10A cells, maximum % cytotoxicity of 85±0.04% was observed at a concentration of 80 µg/mL, and

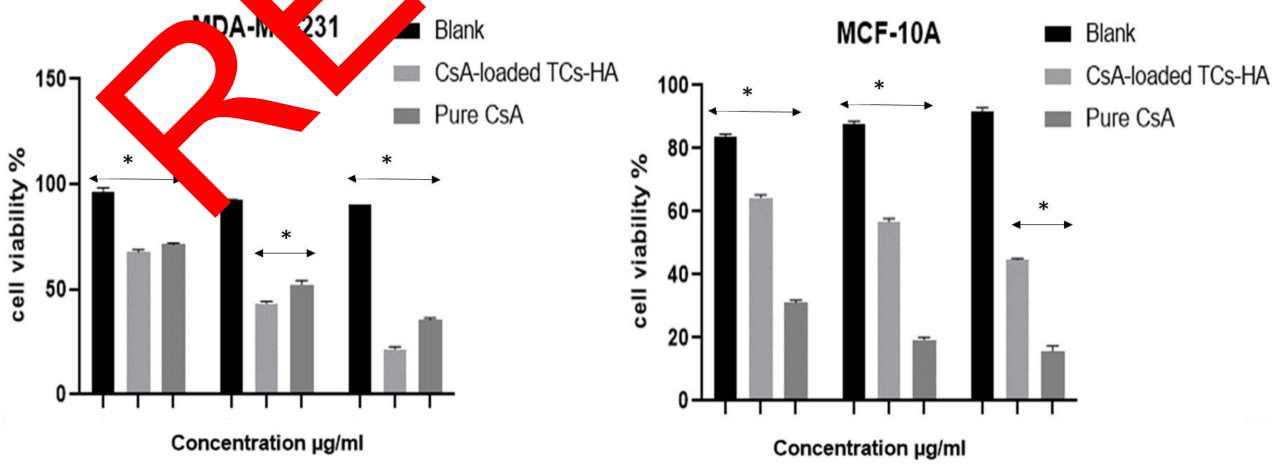

Figure 9 Cell viability analysis by MTT assay outcomes of MDA-MB-231 and MCF-10A cells after treatment with CsA and CsA-NF (mean + SD, *p ≤ 0.05).

Table 7 Trypan Blue Exclusion Result of % Cytotoxicity

S.No	Concentration	CsA-ThC-HA (Mean + SD)	Pure CsA (Mean + SD)
%Cytotoxicity MDA-MB-231			
1	80 µg/mL	85±0.04	79.2±0.07
2	40 µg/mL	60.3±0.21	53.6±0.04
3	10 µg/mL	35.3±0.03	32.1±0.12
4	0 µg/mL	10±0.07	11±0.04
%Cytotoxicity MCF-10A			
1	80 µg/mL	25±0.03	67±0.02
2	40 µg/mL	18.4±0.02	46±0.03
3	10 µg/mL	12±0.05	29.7±0.0
4	0 µg/mL	10±0.07	1±0.

minimum cell viability of 10±0.07% was observed at a concentration of µg/mL for CsA-ThC-HA treated cells. Figure 10 shows the change in cell viability of treated cells in and dose-dependent manner.

Cell Morphology Analysis for Cytopathic Effect

Normal breast epithelial cells MCF-10A and triple-negative breast cancer cells MDA-MB-231 were when treated with different pure CsA and CsA-NF at different concentrations (20 µg/mL, 60 µg/mL, and 90 µg/mL), the cytopathic effect increased in a dose-dependent manner. The cytopathic effect was determined by observing the hallmarks of apoptosis, such as shrunken cells and nuclei, rounding, disaggregation of cells, and loss of characteristic cell morphology. The highest cytopathic effect (CPE) cytopathic effect on MDA-MB-231 cells was seen with CsA-NF, which was comparably significant compared to the effect produced by CsA as shown in Figure 10. Con-versely, the highest CPE on MCF-

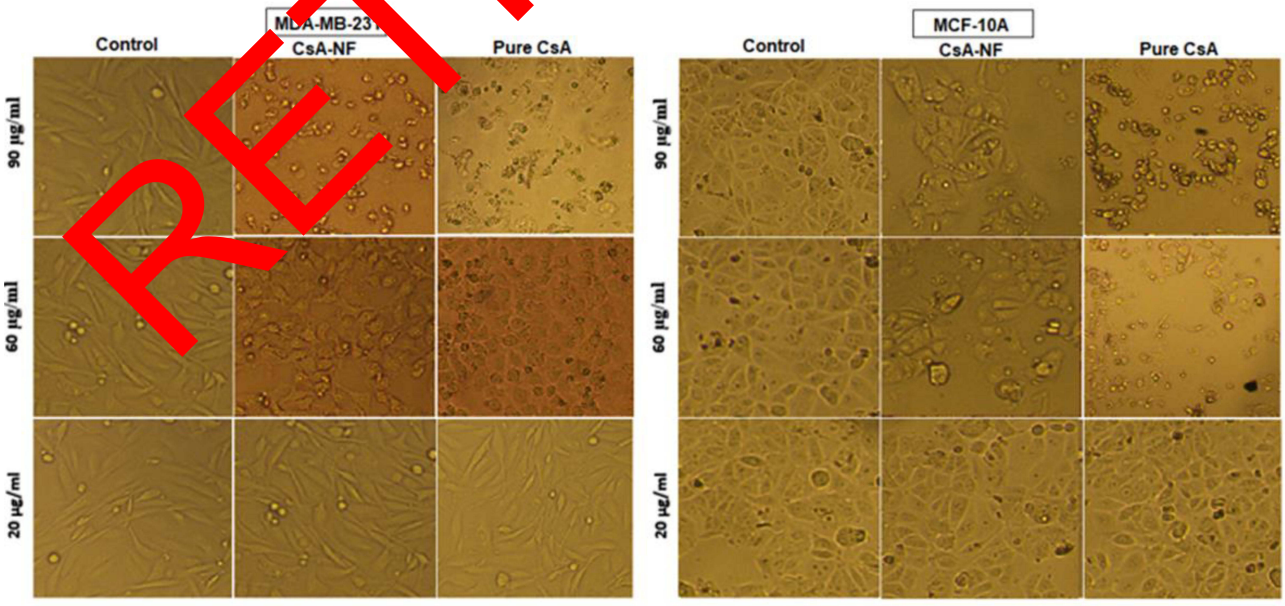

Figure 10 Cell morphology analysis of CsA and CsA-NF treated MDA-MB-231 and MCF-10A cells at 20x magnification.

10A cells was seen with Pure CsA treatment at 80 µg/mL concentration, while CsA-NF did not have much cytopathic effect on MCF-10A cells.

Conclusion

To improve the effectiveness of chemotherapeutics with ligand surface alteration, the current research significantly developed the Cyclosporine loaded in thiolated chitosan (ThC) and encapsulated with Hyaluronic acid (HA) nanoformulation (NF) for the targeted administration of drugs. Considering its hydrophilic properties, pseudo-immunogenicity, longevity, and capacity to carry numerous readily alterable functional groups, HA was selected as the ligand for administering chemotherapy Cyclosporine enclosed in the naturally occurring polymeric compound ThC. The outer shell of the NF was infused with HA, a proven CD44 ligand, for targeted inhibition of the CD44 receptor, which is highly expressed in numerous malignancies, including triple-negative breast cancer. To evaluate the produced NF's effectiveness in-vitro, human triple-negative breast cancer cells and normal breast epithelial cells were used. The nanoparticles were developed with a positive zeta potential which promotes absorption and particle size in the 200–300 range. In addition, using a simplified diffusion model, NFs exhibited considerable cytotoxicity compared to widely accessible Cyclosporine ($p < 0.05$) with a great release trajectory. All of these attributes substantially improve the pharmacokinetic characteristics, effectiveness, and targeted delivery of NFs as a possible localized therapeutic constituent in cancer therapy. Moreover, in-vivo testing of these formulations is required in considering these results.

Data Sharing Statement

Data sharing is not applicable to this article as no datasets were generated or analyzed during the current study.

Institutional Review Board Statement

The used cell lines had ethical or institutional review board approval.

Acknowledgments

The authors gratefully acknowledge the technical and financial support provided by the Ministry of Education and King Abdulaziz University, DSR, Jeddah, Saudi Arabia.

Funding

This research work was funded by Institutional Fund Projects under grant no. (IFPIP: 824-290-1442). Therefore, authors gratefully acknowledge technical and financial support from the Ministry of Education and King Abdulaziz University, DSR, Jeddah, Saudi Arabia.

Disclosure

The author declares no conflicts of interest.

References

1. Terkelsen T, Russo S, Gromov P, et al. Secreted breast tumor interstitial fluid microRNAs and their target genes are associated with triple-negative breast cancer, tumor grade, and immune infiltration. *Breast Cancer Res*. 2020;22(1):1–36. doi:10.1186/s13058-020-01295-6
2. Bou Zerdan M, Ghorayeb T, Saliba F, et al. Triple-negative breast cancer: updates on classification and treatment in 2021. *Cancers*. 2022;14:1253. doi:10.3390/cancers14051253
3. Ismail A, El-Mahdy HA, Abulsoud AI, et al. Beneficial and detrimental aspects of miRNAs as chief players in breast cancer: a comprehensive review. *Int J Biol Macromolecules*. 2022:67.
4. Cuthbert RJ, Russell NH, Jones PA, Morgan AG. Treatment of acute myeloid leukaemia in a renal allograft recipient: implications of cyclosporin immunosuppressive treatment. *J Clin Pathol*. 1991;44:693–695. doi:10.1136/jcp.44.8.693
5. Hoang DM, Pham PT, Bach TQ, et al. Stem cell-based therapy for human diseases. *Signal Transduction Targeted Therapy*. 2022;7:272. doi:10.1038/s41392-022-01134-4
6. Hao W, Cui Y, Fan Y, et al. Hybrid membrane-coated nanosuspensions for multi-modal anti-glioma therapy via drug and antigen delivery. *J Nanobiotechnol*. 2021;19(1):1–24. doi:10.1186/s12951-021-01110-0
7. Guo X, Wei X, Chen Z, Zhang X, Yang G, Zhou S. Multifunctional nanoplatforms for subcellular delivery of drugs in cancer therapy. *Progress Materials Sci*. 2020;107:100599.

8. Tong X, Pan W, Su T, Zhang M, Dong W, Qi X. Recent advances in natural polymer-based drug delivery systems. *Reactive Functional Polymers*. 2020;148:104501. doi:10.1016/j.reactfunctpolym.2020.104501
9. Naseer F, Ahmad T, Kousar K, Kakar S, Gul R, Anjum S. Formulation of surface-functionalized hyaluronic acid-coated thiolated chitosan nanoformulation for the delivery of vincristine in prostate cancer: a multifunctional targeted drug delivery approach. *J Drug Delivery Sci Technol*. 2022;74:103545. doi:10.1016/j.jddst.2022.103545
10. Pillai CKS, Paul W, Sharma CP. Chitosan: manufacture, properties and uses. *Chitosan*. 2011;133–216.
11. Mohammad F, A. Al-Lohedan H, N. Al-Haque H. Chitosan-mediated fabrication of metal nanocomposites for enhanced biomedical applications. *Adv Materials Lett*. 2017;8(2):89–100. doi:10.5185/amlett.2017.6925
12. Kousar K, Naseer F, Abduh MS, et al. Green synthesis of hyaluronic acid coated, thiolated chitosan nanoparticles for CD44 targeted delivery and sustained release of Cisplatin in cervical carcinoma. *Front Pharmacol*. 2022;13.
13. Sarkar SD, Farrugia BL, Dargaville TR, Dhara S. Physico-chemical/biological properties of tripolyphosphate cross-linked chitosan based nanofibers. *Materials Sci Eng C*. 2013;33(3):1446–1454. doi:10.1016/j.msec.2012.12.066
14. Narmani A, Jafari SM. Chitosan-based nanodelivery systems for cancer therapy: recent advances. *Carbohydrate Polymers*. 2021;272:118464. doi:10.1016/j.carbpol.2021.118464
15. Luo M, Wicha MS. Targeting cancer stem cell redox metabolism to enhance therapy responses. *Proce Semi Radiat Oncol*. 2019;29(1):42–54. doi:10.1016/j.semradonc.2018.10.003
16. Mattheolabakis G, Milane L, Singh A, Amiji MM. Hyaluronic acid targeting of CD44 for cancer therapy: from receptor biology to nanomedicine. *J Drug Targeting*. 2015;23(7–8):605–618. doi:10.3109/1061186X.2015.1052072
17. Uz Zaman S, Arshad R, Tabish TA, Naseem AA, Shahnaz G. others Mapping the potential of thiolated hyaluronic based nanomicelles for the safe and targeted delivery of vancomycin against staphylococcal blepharitis. *J Drug Delivery Sci Technol*. 2021;61:102220. doi:10.1016/j.jddst.2020.102220
18. Anitha A, Deepa N, Chennazhi KP, Nair SV, Tamura H, Jayakumar R. Development of mucoadhesive thiolated chitosan nanoparticles for biomedical applications. *Carbohydrate Polymers*. 2011;83(1):66–73. doi:10.1016/j.carbpol.2010.07.028
19. Wang Y, Cai H, Naviner LAB, et al. A process-variation-resilient methodology of circuit design by the asymmetric forward body bias in 28 nm FDSOI. *Microelectronics Reliability*. 2016;64:26–30. doi:10.1016/j.microrel.2016.07.073
20. Silvestro I, Francolini I, Di Lisio V, Martinelli A, Pietrelli L. Preparation and characterization of TPP-chitosan crosslinked scaffolds for tissue engineering. *Materials*. 2020;13(16):3577. doi:10.3390/ma13163577
21. Mukhtar M, Pallagi E, Csóka I, et al. Aerodynamic properties and in silico deposition of isoniazid loaded chitosan/thiolated chitosan and hyaluronic acid hybrid nanoplex DPIs as a potential TB treatment. *Int J Biol Macromolecules*. 2020;165:3003–3019. doi:10.1016/j.ijbiomac.2020.10.192
22. Yanat M, Schroën K. Preparation methods and applications of chitosan nanoparticles; with an outlook toward reinforcement of biodegradable packaging. *Reactive Functional Polymers*. 2021;161:104849. doi:10.1016/j.reactfunctpolym.2021.104849
23. Jalilian M, Derakhshandeh K, Kurd M, Lashani H. Targeting Solid Lipid Nanoparticles with Anisamide for Docetaxel Delivery to Prostate Cancer: preparation, Optimization, and In-vitro Evaluation. *Iranian J Pharm Res*. 2021;20:327. doi:10.22037/ijpr.2020.113436.14302
24. Ghaferi M, Amari S, Vivek Mohrir B, Raza A, Ebrahimi Shafiee M, Alavi SE. Preparation, characterization, and evaluation of cisplatin-loaded polybutylcyanoacrylate nanoparticles with improved in vitro and in vivo anticancer activities. *Pharmaceuticals*. 2020;13(3):44. doi:10.3390/ph13030044
25. Bhattacharya DS, Svechkarev D, Souchek JJ, et al. Impact of structurally modifying hyaluronic acid on CD44 interaction. *J Materials Chem B*. 2017;5:8183–8192. doi:10.1039/C7TB01895A
26. Nur SG, Buket O, Sezgi K, et al. Synthesis of methotrexate loaded chitosan nanoparticles and in vitro evaluation of the potential in treatment of prostate cancer. *Anti-Cancer Agents Medicinal Chem*. 2018;18(8):1038–1042. doi:10.2174/1871520616666160101120040
27. Kumar N, Salar RK, Prasad M, Ranjan K. Synthesis, characterization and anticancer activity of vincristine loaded folic acid-chitosan conjugated nanoparticles on NCI-H460 non-small cell lung cancer cell line. *Egyptian J Basic Appl Sci*. 2018;5(1):87–99. doi:10.1016/j.ejbas.2017.11.002
28. Danaei M, Dehghankhold M, Ataei S, et al. Impact of particle size and polydispersity index on the clinical applications of lipidic nanocarrier systems. *Pharmaceutics*. 2018;10(2):57. doi:10.3390/pharmaceutics10020057
29. Maeda H, Wu J, Sawa T, Matsumura Y, Hori K. Tumor vascular permeability and the EPR effect in macromolecular therapeutics: a review. *J Controlled Release*. 2000;65(1–2):271–284. doi:10.1016/S0168-3659(99)00248-5
30. Maria S, Sarwar H, Sohail M, et al. Synthesis and characterization of pre-activated thiolated chitosan nanoparticles for oral delivery of octreotide. *J Drug Delivery Sci Technol*. 2020;58:101807. doi:10.1016/j.jddst.2020.101807
31. Wang T, Hou J, Su C, Zhao L, Shi Y. Hyaluronic acid-coated chitosan nanoparticles induce ROS-mediated tumor cell apoptosis and enhance antitumor efficacy by targeted drug delivery via CD44. *J Nanobiotechnol*. 2017;15(1):1–12. doi:10.1186/s12951-016-0245-2
32. Nakamura H, Watano S. Direct permeation of nanoparticles across cell membrane: a review. *KONA Powder Particle J*. 2018;2018011.
33. Sahu A, Ratre YK, Chauhan S, Bhaskar L, Nair MP, Verma HK. Nanotechnology based drug delivery system: current strategies and emerging therapeutic potential for medical science. *J Drug Delivery Sci Technol*. 2021;63:102487. doi:10.1016/j.jddst.2021.102487
34. Anitha A, Sowmya S, Deepa N, Chennazhi KP, Nair SV, Jayakumar R. Curcumin-loaded N, O-carboxymethyl chitosan nanoparticles for cancer drug delivery. *J Biomaterials Sci Polymer Edition*. 2012;23:1381–1400. doi:10.1163/092050611X581534
35. Eliezar J, Scaramuzza W, Boase NRB, Thurecht KJ, Stenzel MH. In vivo evaluation of folate decorated cross-linked micelles for the delivery of platinum anticancer drugs. *Biomacromolecules*. 2015;16:515–523. doi:10.1021/bm501558d
36. Shahnaz G, Edagwa BJ, McMillan J, et al. Development of mannose-anchored thiolated amphotericin B nanocarriers for treatment of visceral leishmaniasis. *Nanomedicine*. 2017;12(2):99–115. doi:10.2217/nnm-2016-0325
37. Oh J-W, Chun SC, Chandrasekaran M. Preparation and in vitro characterization of chitosan nanoparticles and their broad-spectrum antifungal action compared to antibacterial activities against phytopathogens of tomato. *Agronomy*. 2019;9(1):21. doi:10.3390/agronomy9010021
38. Petschauer JS, Madden AJ, Kirschbrown WP, Song G, Zamboni WC. The effects of nanoparticle drug loading on the pharmacokinetics of anticancer agents. *Nanomedicine*. 2015;10(3):447–463. doi:10.2217/nnm.14.179
39. Xu S, Xu Q, Zhou J, Wang J, Zhang N, Zhang L. Preparation and characterization of folate-chitosan-gemcitabine core–shell nanoparticles for potential tumor-targeted drug delivery. *J Nanosci Nanotechnol*. 2013;13:129–138. doi:10.1166/jnn.2013.6794
40. Wang W, Tong C, Liu X, Li T, Liu B, Xiong W. Preparation and functional characterization of tumor-targeted folic acid-chitosan conjugated nanoparticles loaded with mitoxantrone. *J Central South Univ*. 2015;22(9):3311–3317. doi:10.1007/s11771-015-2871-5